Showcasing research from Professor Balkus' Lab, Department of Chemistry and Biochemistry, The University of Texas at Dallas, Richardson, Texas USA.

Fluorine extraction from organofluorine molecules to make fluorinated clusters in yttrium MOFs

Rare-earth metal-organic frameworks (MOFs) have been investigated for biomedical, magnetic, and optical properties. We recently discovered that fluorine can be extracted from various organic molecules to form fluoro-bridged MOFs. A new yttrium MOF is reported with fluorinated clusters. Moreover, it is demonstrated that pollutants such as PFAS can be destroyed during the MOF synthesis to make the fluorinated clusters. The presence of fluorinated clusters in the MOFs is expected to improve the fluorescence, magnetic and separation properties.

As featured in:

See Kenneth J. Balkus *et al.*,
Chem. Sci., 2022, **13**, 14285.

ROYAL SOCIETY OF CHEMISTRY

rsc.li/chemical-science

ROYAL SOCIETY OF CHEMISTRY

Fluorine extraction from organofluorine molecules to make fluorinated clusters in yttrium MOFs†

Muhammad Abbas, [a] Amanda M. Maceda, [a] Hamid R. Firouzi, [a] Zhifeng Xiao, [b] Hadi D. Arman, [c] Yanshu Shi, [c] Hong-Cai Zhou [b] and Kenneth J. Balkus, Jr [*a]

A new rare earth based two-dimensional coordination network and a three-dimensional metal–organic framework (MOF) have been synthesized using bicinchoninic acid (BCA) and yttrium(III) ions. Yttrium dimer nodes are formed in the absence of a modulator, resulting in a 2D layered coordination network (**Y−BCA-2D**). The presence of fluorinating agents, *e.g.*, 2-fluorobenzoic acid (2-FBA), 2,6-difluorobenzoic acid (2,6-DFBA), and perfluorohexanoic acid (PFHxA) result in μ_3-F bridged metal hexaclusters (Y_6F_8) that form a three-dimensional MOF (**Y−BCA-3D**). It was found that Y^{3+} can break highly stable C–F bonds in aromatic and aliphatic fluorinated compounds. Single-crystal X-ray diffraction (SC-XRD) shows the presence of fluorine in the metal cluster which was confirmed by energy dispersive X-ray spectroscopy (EDS). High resolution X-ray photoelectron spectroscopy (XPS) and ^{19}F Nuclear Magnetic Resonance (NMR) also verify the presence of metal–fluorine bonds in the cluster. The **Y−BCA-3D** MOF selectively adsorbs CO_2 but not N_2.

Introduction

Metal–organic frameworks (MOFs) are crystalline hybrid organic–inorganic compounds that have been used in a variety of applications including conductive materials,[1–3] catalysis,[4–9] drug delivery,[10] radio therapy,[11–13] water harvesting,[14,15] gas storage, and separations.[16–19] There is growing interest in rare-earth (RE) MOFs, particularly due to their high coordination number (CN: 6–12), magnetic properties, optical properties, and therapeutic applications.[20–25] The RE metal ions tend to form dimers that often result in MOFs with low porosity.[26–28] It has been widely reported that the addition of a modulator can result in RE-MOFs with larger metal clusters.[29–32] Modulators were originally designed to bind to metal ions to control crystallization rates, often leading to larger X-ray quality crystals.[33,34] A popular modulator is 2-fluorobenzoic acid (2-FBA) (Fig. 1).[35–38] This molecule has been used to synthesize RE based MOFs where the metal nodes have been reported to be hydroxo (μ_3-OH$^-$) bridged hexanuclear clusters.[35–54] In contrast, it was found that in the case of Ho^{3+} and terephthalic acid (BDC), the addition of 2-FBA to the synthesis resulted in a fluoro-bridged

hexanuclear cluster in a UiO-66 analog.[55] Additionally, it was found that Ho^{3+} could extract fluorine from 2-FBA and form HoF$_3$. The presence of fluorine in metal clusters can also improve their thermodynamic stability compared to hydroxy bridged clusters.[56] Fluorinated metal clusters are hydrophobic and can improve the water stability of the MOFs.[57] The fluorine in the clusters may improve the framework interaction with CO_2 that can be exploited in separations. For example, the Y-MOF in a recent mixed matrix membrane that showed enhanced CO_2 separation is likely a fluorinated MOF.[55,58] Fluorinated RE clusters exhibit enhanced photoluminescence which may also be the case in fluorinated RE-MOFs.[59]

Perfluoroalkyl and polyfluoroalkyl substances (PFAS) are highly stable compounds used in a variety of coating applications, such as heat-resistant non-stick utensils, hydrophobic packaging, adhesives, and furniture surfacing.[60,61] These compounds are remarkably stable under high temperatures, extreme chemical conditions, and in both hydrophilic and hydrophobic environments.[62] The aliphatic C–F bonds are very

a Department of Chemistry and Biochemistry, The University of Texas at Dallas, 800 West Campbell Rd, Richardson, TX 75080, USA. E-mail: balkus@utdallas.edu

b Department of Chemistry, Texas A&M University, College Station, TX 77843, USA

c Department of Chemistry, University of Texas at San Antonio, One UTSA Circle, San Antonio, Texas 78249, USA

† Electronic supplementary information (ESI) available. CCDC 2206798 (**Y−BCA-2D**), and 2207094 (**Y-3D-MOF**). For ESI and crystallographic data in CIF or other electronic format see DOI: https://doi.org/10.1039/d2sc05143e

Fig. 1 Structures of 2-fluorobenzoic acid (2-FBA), 2,6-difluorobenzoic acid (2,6-DFBA), and perfluorohexanoic acid (PFHxA).

Fig. 2 Structures of organic linkers [2,2′-bipyridine]-4,4′-dicarboxylic acid (BPDC), and bicinchoninic acid (BCA).

Fig. 3 Structure of **Y–BCA-2D** (a) cluster structure with metal-dimer node, (b) layered structure, and (c) topological representation showing a single layer and stacking.

stable with a bond dissociation energy exceeding 500 kJ mol^{-1}.[63,64] According to the Centers for Disease Control and Prevention (CDC) and the United States Environmental Protection Agency (EPA), PFAS contamination in soil and drinking water are becoming a serious environmental threat.[60,65] In this study, it is found that Y^{3+} can break C–F bonds in organo-fluorine molecules including perfluorohexanoic acid (PFHxA) and form YF$_3$ or fluoro-bridged hexaclusters in a new MOF, **Y–BCA-3D**.

A fluorine-bridged trinuclear cluster was formed with the organic linker [2,2′-bipyridine]-4,4′-dicarboxylic acid (BPDC) (Fig. 2).[55] In the present work, the linker BCA (Fig. 2) was used to make a new MOF using Y^{3+}. Similar to Ho^{3+}, the Y^{3+} ion extracts fluorine from 2-FBA, 2,6-DFBA, as well as PFHxA (Fig. 1). In the absence of an organo-fluorine molecule, a new two-dimensional MOF (**Y–BCA-2D**) was formed. The 2D and 3D MOFs were characterized by thermogravimetric analysis (TGA), EDS, XPS, XRD, ^{19}F-NMR and gas sorption analysis (N$_2$, CO$_2$).

Results and discussion

In the absence of fluorinated modulators, the solvothermal reaction of Y(NO$_3$)$_3$·6(H$_2$O) with the BCA ligand yielded a two-dimensional MOF, [Y$_2$(μ$_4$-BCA)$_2$(μ$_3$-BCA)$_4$(DMF)$_4$]$_n$·nDMF·n(H$_2$O) (**Y–BCA-2D**). Single-crystal XRD (SC-XRD) analysis reveals that **Y–BCA-2D** crystalizes into a triclinic space group, P$\bar{1}$. The Y^{3+} has a coordination number of nine in the **Y–BCA-2D** dimer node. In the structure of **Y–BCA-2D**, inversion centers lie at the center of the Y-based binuclear clusters as shown in Fig. 3(a). In these binuclear clusters, each Y center is coordinated to two terminal DMF molecules by the carbonyl oxygen atoms and eight carboxylate groups from the BCA ligands. There are two types of chemically distinct BCA ligands in the structure, namely type-1 and type-2 as shown in Fig. S1(a).† Each type-1 BCA ligand has one η^2-carboxylate group chelating to a Y^{3+} ion and another μ$_2$, η^3-carboxylate group bridging the Y^{3+} ions in the binuclear clusters. Type-2 BCA ligands are geometrically perpendicular to the type-1 BCA ligands. Each BCA linker is bound to four different Y^{3+} ions from two different binuclear clusters by its two bridging carboxylate groups. In the extended structure of **Y–BCA-2D**, two

type-1 BCA ligands pair up and align in an antiparallel fashion, connecting two adjacent binuclear clusters and forming an infinite chain as shown in Fig. 3(b). Perpendicular to this chain, type-2 BCA ligands forms another infinite chain while connecting the binuclear clusters in proximity. Topologically, the two perpendicular chains generate a two-dimensional 4-c net with the sql topology as shown in the Fig. 3(c). The 2D layers are aligned in a staggered configuration with the clusters being on top of the type-2 BCA ligands from an adjacent layer (Fig. S1†). The staggering alignment of these layers leads to elimination of pore space with a minimal Platon void percentage of 3%. Between each layer, there are DMF, and water molecules as shown in Fig. S1.† The crystal packing of the 2-dimensional layers is further highlighted in Fig. S2,† where alternate layers are colored green and purple, and solvent molecules are removed for clarity. The phase purity of the product was confirmed by powder XRD (Fig. S6†).

In the presence of fluorinated modulators (2-FBA, 2,6-DFBA, PFHxA), the solvothermal reaction of Y(NO$_3$)$_3$·6(H$_2$O) with the BCA ligand yielded a three-dimensional MOF (**Y–BCA-3D**) with an empirical formula of C$_{30}$H$_{15}$F$_2$N$_3$O$_{6.62}$Y$_{1.5}$. **Y–BCA-3D** crystalized in the tetragonal space group I4/m. The crystal structure of **Y–BCA-3D** consists of yttrium hexanuclear clusters coordinated by BCA linkers. Yttrium has the same coordination number (i.e., CN: 9) as in the dimer, but the μ$_3$-F bridges form a hexanuclear cluster (Y$_6$F$_8$), as shown in Fig. 4(a and b). Each hexanuclear cluster is connected to BCA linkers via η^2-carboxylate groups. Each Y^{3+} ion is coordinated with one water molecule, four μ$_3$-F, and four oxygen atoms from carboxylate groups. The extended network shows that **Y–BCA-3D** has the same fcu topology as the UiO-66 Fig. 4(c and d).[66] Details of the crystallographic data collection and instrumentation are discussed in the ESI† as well as the crystal parameters, and refinement details are given in Table S1.† The powder XRD confirms the crystallinity and bulk purity of the product when compared to the simulated pattern from the single crystal structure (Fig. S6†).

Fig. 4 Crystal structure of **Y–BCA-3D** (a) cluster structure with hexanuclear node, (b) *c*-axis view of hexacluster and isolated Y_6F_8 cluster, (c) extended 3D network view along the *a*-axis showing 6.3 Å spherical cavities (purple), and (d) underlying net topology of the MOF viewed along the *a*-axis.

The formation of these μ_3-F bridged hexaclusters depends on the nature of the modulator and the ratio with the BCA linker. It was found that 2-FBA gave a mixture of 2D/3D MOFs if used in a modulator/BCA mole ratio less than 15. While the same ratios of 2,6-DFBA and PFHxA only form the hexaclusters. This could reflect the lower pK_a of BCA (1.77), which competes with the modulator for the Y^{3+} ions. The pK_a values for the modulators are 3.27, 2.34, and −0.15 for 2-FBA, 2,6-DFBA, and PFHxA, respectively. The ideal linker to modulator mole ratios were found as 1 : 18, 1 : 14, and 1 : 7 for 2-FBA, 2,6-DFBA, and PFHxA, respectively. It should be noted that an excess amount of modulator in all cases resulted in a mixture of YF_3 and **Y–BCA-3D**. Therefore, the donor strength of the modulator *versus* the linker must be taken into careful consideration when designing fluoro-bridged RE-MOFs. Attempts to use NaF and NH_4F as the fluorine source in the synthesis of **Y–BCA-3D** only resulted in formation of yttrium fluorides. Moreover, attempts to convert the 2D MOF to the 3D MOF by heating with organofluorine modulators only resulted in formation of YF_3.

The EDS elemental mapping confirms the presence of fluorine in the **Y–BCA-3D**. The EDS of **Y–BCA-3D** synthesized with different fluorinated modulators show that the amount of fluorine is consistent with the theoretically calculated amount (Fig. S3–S5†).

Fluorine nuclear magnetic resonance (^{19}F-NMR) spectroscopy was used to confirm the presence of fluorine in the MOFs. Three different samples of **Y–BCA-3D** synthesized using different fluorinated modulators *i.e.*, 2-FBA, 2,6-DFBA, and PFHxA were digested in 10% deuterated sulfuric acid. A comparison of ^{19}F-NMR spectra for modulators and digested **Y–BCA-3D** MOFs is shown in Fig. S7–S9.† ^{19}F-NMR spectra of acid digested **Y–BCA-3D** confirmed that there were no trapped modulators inside the MOF pores, as the fluorine chemical shifts do not match the modulators. The chemical shift peaks at −169 ppm correspond to hydrofluoric acid (HF) formed by the release of bridging fluorine from the digested MOF, as these peaks are in the same region as the reported ^{19}F-NMR peak for HF.[67,68]

It should be noted that the only source of fluorine was the organo-fluorine molecules (2-FBA, 2,6-DFBA, or PFHxA). It was confirmed that the fluorine in the **Y–BCA-3D** is present in the metal nodes, and not unreacted or trapped organo-fluorine molecules. As a proof of fluorine extraction, a reaction of just the modulator and Y^{3+} was carried out without the organic linker. The Y^{3+} can extract fluorine from 2-FBA, 2,6-DFBA and PFHxA to make YF_3 (Fig. S10†). The formation of YF_3 was confirmed by comparing the powder XRD with its simulated pattern, and no impurities were found (Fig. S11†).[69]

Fig. 5 The XPS spectra of (a) Y–BCA-3D survey, (b) Y–BCA-3D high resolution Y $3d_{5/2}$ and $3d_{3/2}$, (c) Y–BCA-2D survey, and (d) Y–BCA-2D high resolution Y $3d_{5/2}$ and $3d_{3/2}$.

The presence of elemental chemical states can be precisely determined by the XPS. The survey spectra of the 2D and 3D MOFs shown in Fig. 5(a and c) confirms the presence of yttrium, fluorine, and BCA linker elements *i.e.*, carbon, nitrogen, and oxygen. The high-resolution spectrum of **Y–BCA-3D** gave spin–orbit coupled peaks of Y $3d_{5/2}$ and $3d_{3/2}$ at 158.2 eV and 160.2 eV, respectively. The **Y–BCA-2D** shows a binding energy (BE) of Y $3d_{5/2}$ at 157.4 eV. As, **Y–BCA-2D** only has yttrium–oxygen bonds, similar to Y_2O_3.[70] Whereas, the BE of Y $3d_{5/2}$ in YF_3 is 159 eV due to Y–F bonds. In the case of **Y–BCA-3D**, these energies correspond to yttrium bound to oxygen and fluorine (O–Y–F) in the hexacluster. Hence, the Y $3d_{5/2}$ BE in the hexacluster is in between the Y_2O_3 and YF_3.

The F 1s high resolution XPS spectra show the BE for C–F in 2-FBA, 2,6-DFBA and PFHxA as 686.7, 687.5, and 689.2 eV, respectively (Fig. 6(a–c)). Whereas the **Y–BCA-3D** shows a peak at 684.7 eV, which corresponds to fluorine bound to yttrium. This can be compared to YF_3 at 685.1 eV for F 1s. The F 1s spectrum for a physical mixture of **Y–BCA-3D** and 2,6-DFBA was recorded. Fig. 6(f) shows that the mixture has two distinct chemical states of fluorine with binding energies at 684.7 and 687.5 eV for Y–F and C–F, respectively. Hence, it can be concluded that the fluorine is bound to yttrium in the hexacluster, and no free organic fluorine is present in the **Y–BCA-3D**.

Thermogravimetric analysis of the MOFs activated at 160 °C under vacuum shows that the 2D-MOF decomposes around 460 °C in air and at 500 °C under a nitrogen atmosphere. Whereas the pristine BCA linker decomposes at 300 °C under air (Fig. S12†). The **Y–BCA-2D** structure loses 5% mass around 100 °C and is assigned to the loss of adsorbed water. A further 5% mass loss at 300 °C is assigned to coordinated DMF. Similarly, the 3D-MOF also has superior stability in comparison to the BCA linker and stable up to 450 °C. It gave a 7% weight loss at 100 °C for trapped water molecules, which show that it has relatively more free volume in comparison to **Y–BCA-2D**.

The porosity of the MOFs was probed using ultra high purity nitrogen and carbon dioxide. The nitrogen adsorption–desorption analysis shows that the activated **Y–BCA-2D** is a densely packed material with a very low BET surface area of 11.5 m^2 g^{-1}. Whereas, the CO_2 adsorption data shows a surface area of 33.1 m^2 g^{-1} that indicates the presence of some microporosity. Similarly, the nitrogen adsorption isotherm for **Y–BCA-3D** MOF shows a surface area of 5.7 m^2 g^{-1} and 94.5 m^2 g^{-1} for the CO_2 adsorption isotherm. The surface area for the similar linker *i.e.*, BPDC (Fig. 2) in a Gd-trinuclear cluster-based MOF is 177.7 m^2 g^{-1}. This shows that the **Y–BCA-3D** has less surface area, but it is selective for CO_2
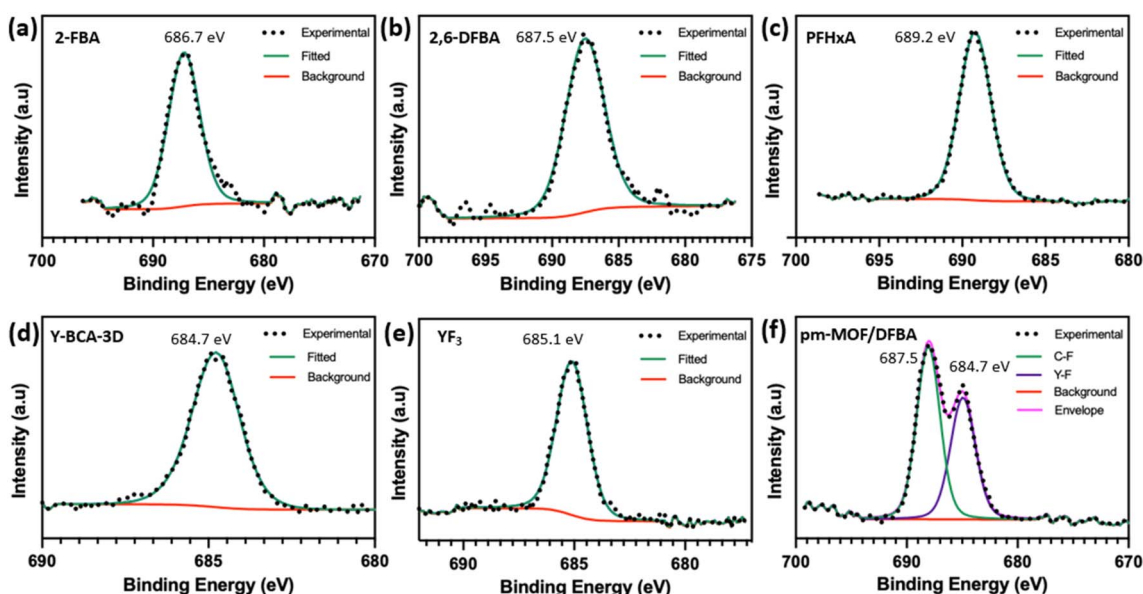

Fig. 6 High resolution F 1s XPS spectra of (a) 2-FBA, (b) 2,6-DFBA, (c) PFHxA, (d) Y–BCA-3D, (e) YF$_3$, and (f) physical mixture of **Y–BCA-3D** and 2,6-DFBA.
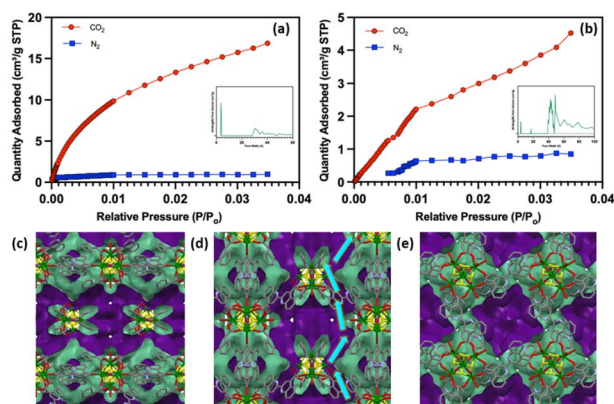
Fig. 7 Adsorption isotherms for (a) Y–BCA-3D and (b) Y–BCA-2D. Representation of sinusoidal voids/channels (purple) in Y–BCA-3D (c) viewed along *a*-axis, (d) viewed along *b*-axis and gas passage is highlighted by arrows, and (e) viewed along *c*-axis show presence of deep spherical cavities with a diameter of 6.3 Å.

uptake due to its narrow pore openings. Even though Fig. 7(c) show that **Y–BCA-3D** has 6.3 Å spherical cavities, bigger than the kinetic diameter of nitrogen (3.64 Å), it does not allow N_2 adsorption. The calculated void spaces show that the channels are zigzag along *a* and *b*-axes (Fig. 7(c–e)). These channels have narrow openings ∼4 Å along the *a* and *b*-axes and have deep spherical cage type 6.3 Å cavities along *c*-direction. These cavities dead end along the *c*-axis but are accessible through the *a* and *b*-axes. This was experimentally verified by the pore volume calculated by gas sorption data as shown in Fig. 7(a and b).

Conclusions

The extraction of fluorine from various organo-fluorine compounds by rare earth metal ions has opened up a new area for MOFs synthesis. A new yttrium MOF with the BCA linker features a fluorine bridged hexacluster. The Y^{3+} ions can extract fluorine from aromatic and aliphatic carbons. This work is currently being extended to other rare earth metal ions, as different RE metals exhibit various fluorine affinities. Understanding how the fluorine affinities play a role in the cluster formation can provide insights into the design of these MOFs as well as their potential application in fluorine sensing and extraction. The fluorine bridges found in these clusters are expected to have an effect on the optical properties of the MOFs, and those studies are in progress.

Data availability

CCDC numbers 2206798 (**Y–BCA-2D**), and 2207094 (**Y-3D-MOF**). Additional experimental details and data are provided in the ESI,† including NMR, EDS, TGA, PXRD, optical images, and crystallographic data.

Author contributions

KJB and MA conceived and designed the project. MA performed experiments, analyzed the materials by PXRD, XPS, TGA, SEM, gas sorption, and wrote the original draft. AMM helped in setting up reactions carried PXRD and edited draft. HRF carried NMR studies. ZX, HDA and YS carried out SC-XRD analysis, HZ and KJB provided resources. KJB funding acquisition, conceptualization, review and editing, supervision, and project administration. All authors have given approval to the final version of the manuscript.

Conflicts of interest

The authors declare no competing financial interest.

References

1 J. Y. Choi, J. Flood, M. Stodolka, H. T. B. Pham and J. Park, *ACS Nano*, 2022, **16**, 3145–3151.
2 G. Skorupskii, K. N. Le, D. L. M. Cordova, L. Yang, T. Chen, C. H. Hendon, M. Q. Arguilla and M. Dincă, *Proc. Natl. Acad. Sci. U. S. A.*, 2022, **119**, e2205127119.
3 M. de Lourdes Gonzalez-Juarez, C. Morales, J. I. Flege, E. Flores, M. Martin-Gonzalez, I. Nandhakumar and D. Bradshaw, *ACS Appl. Mater. Interfaces*, 2022, **14**, 12404–12411.
4 L. Zhu, X.-Q. Liu, H.-L. Jiang and L.-B. Sun, *Chem. Rev.*, 2017, **117**, 8129–8176.
5 M. Ahsan Usman, M. Naeem, M. Saeed and M. Zaheer, *Inorg. Chim. Acta*, 2021, **521**, 120305.
6 X. Feng, Y. Song, J. S. Chen, Z. Li, E. Y. Chen, M. Kaufmann, C. Wang and W. Lin, *Chem. Sci.*, 2019, **10**, 2193–2198.
7 J. Huo, J. Aguilera-Sigalat, S. El-Hankari and D. Bradshaw, *Chem. Sci.*, 2015, **6**, 1938–1943.
8 Z. Y. Gu, J. Park, A. Raiff, Z. Wei and H. C. Zhou, *ChemCatChem*, 2014, **6**, 67–75.
9 M. Stodolka and J. Park, *ACS Cent. Sci.*, 2022, **8**, 877–879.
10 Y. Chen, P. Li, J. A. Modica, R. J. Drout and O. K. Farha, *J. Am. Chem. Soc.*, 2018, **140**, 5678–5681.
11 H. D. Lawson, S. P. Walton and C. Chan, *ACS Appl. Mater. Interfaces*, 2021, **13**, 7004–7020.
12 K. Ni, G. Lan, Y. Song, Z. Hao and W. Lin, *Chem. Sci.*, 2020, **11**, 7641–7653.
13 K. Ni, Z. Xu, A. Culbert, T. Luo, N. Guo, K. Yang, E. Pearson, B. Preusser, T. Wu, P. la Riviere, R. R. Weichselbaum, M. T. Spiotto and W. Lin, *Nat. Biomed. Eng.*, 2022, **6**(2), 144–156.

14 M. J. Kalmutzki, C. S. Diercks and O. M. Yaghi, *Adv. Mater.*, 2018, **30**, 1704304.

15 H. Furukawa, F. Gándara, Y.-B. Zhang, J. Jiang, W. L. Queen, M. R. Hudson and O. M. Yaghi, *J. Am. Chem. Soc.*, 2014, **136**, 4369–4381.

16 H. C. Zhou, J. R. Long and O. M. Yaghi, *Chem. Rev.*, 2012, **112**, 673–674.

17 K. Chen, S. H. Mousavi, R. Singh, R. Q. Snurr, G. Li and P. A. Webley, *Chem. Soc. Rev.*, 2022, **51**, 1139–1166.

18 Z. M. Schulte, Y. H. Kwon, Y. Han, C. Liu, L. Li, Y. Yang, A. G. Jarvi, S. Saxena, G. Veser, J. K. Johnson and N. L. Rosi, *Chem. Sci.*, 2020, **11**, 12807–12815.

19 X. Zhao, B. Xiao, A. J. Fletcher, K. M. Thomas, D. Bradshaw and M. J. Rosseinsky, *Science*, 2004, **306**, 1012–1015.

20 F. Saraci, V. Quezada-Novoa, P. R. Donnarumma and A. J. Howarth, *Chem. Soc. Rev.*, 2020, **49**, 7949–7977.

21 V. Trannoy, A. N. Carneiro Neto, C. D. S. Brites, L. D. Carlos, H. Serier-Brault, V. Trannoy, H. Serier-Brault, A. N. C. Neto, C. D. S. Brites and L. D. Carlos, *Adv. Opt. Mater.*, 2021, **9**, 2001938.

22 A. Kourtellaris, W. Lafargue-Dit-Hauret, F. Massuyeau, C. Latouche, A. J. Tasiopoulos and H. Serier-Brault, *Adv. Opt. Mater.*, 2022, 2200484.

23 I. N'Dala-Louika, D. Ananias, C. Latouche, R. Dessapt, L. D. Carlos and H. Serier-Brault, *J. Mater. Chem. C*, 2017, **5**, 10933–10937.

24 G. Skorupskii, K. N. Le, D. L. M. Cordova, L. Yang, T. Chen, C. H. Hendon, M. Q. Arguilla and M. Dincă, *Proc. Natl. Acad. Sci. U. S. A.*, 2022, **119**, e2205127119.

25 T. Feng, Y. Ye, X. Liu, H. Cui, Z. Li, Y. Zhang, B. Liang, H. Li and B. Chen, *Angew. Chem.*, 2020, **132**, 21936–21941.

26 J. P. Vizuet, A. L. Lewis, G. T. McCandless and K. J. Balkus, *J. Nanosci. Nanotechnol.*, 2019, **20**, 3019–3024.

27 J. P. Vizuet, A. L. Lewis, G. T. McCandless and K. J. Balkus, *Polyhedron*, 2019, **159**, 12–17.

28 M. L. Mortensen, A. L. Lewis, G. McCandless and K. J. Balkus, *Crystals*, 2021, **11**, 1547.

29 J. I. Deneff, L. E. S. Rohwer, K. S. Butler, N. R. Valdez, M. A. Rodriguez, T. S. Luk and D. F. Sava Gallis, *ACS Appl. Mater. Interfaces*, 2022, **14**, 3038–3047.

30 N. Wei, R. X. Zuo, Y. Y. Zhang, Z. B. Han and X. J. Gu, *Chem. Commun.*, 2017, **53**, 3224–3227.

31 Y. J. Li, Y. L. Wang and Q. Y. Liu, *Inorg. Chem.*, 2017, **56**, 2159–2164.

32 C. Liu, S. v. Eliseeva, T. Y. Luo, P. F. Muldoon, S. Petoud and N. L. Rosi, *Chem. Sci.*, 2018, **9**, 8099–8102.

33 S. Wannapaiboon, K. Sumida, K. Dilchert, M. Tu, S. Kitagawa, S. Furukawa and R. A. Fischer, *J. Mater. Chem. A*, 2017, **5**, 13665–13673.

34 R. S. Forgan, *Chem. Sci.*, 2020, **11**, 4546–4562.

35 D. Alezi, A. M. P. Peedikakkal, Ł. J. Weseliński, V. Guillerm, Y. Belmabkhout, A. J. Cairns, Z. Chen, Ł. Wojtas and M. Eddaoudi, *J. Am. Chem. Soc.*, 2015, **137**, 5421–5430.

36 V. Guillerm, Ł. J. Weseliński, Y. Belmabkhout, A. J. Cairns, V. D'Elia, Ł. Wojtas, K. Adil and M. Eddaoudi, *Nat. Chem.*, 2014, **6**(8), 673–680.

37 D. X. Xue, Y. Belmabkhout, O. Shekhah, H. Jiang, K. Adil, A. J. Cairns and M. Eddaoudi, *J. Am. Chem. Soc.*, 2015, **137**, 5034–5040.

38 D. X. Xue, A. J. Cairns, Y. Belmabkhout, L. Wojtas, Y. Liu, M. H. Alkordi and M. Eddaoudi, *J. Am. Chem. Soc.*, 2013, **135**, 7660–7667.

39 G. K. Angeli, E. Loukopoulos, K. Kouvidis, A. Bosveli, C. Tsangarakis, E. Tylianakis, G. Froudakis and P. N. Trikalitis, *J. Am. Chem. Soc.*, 2021, **143**, 10250–10260.

40 N. Panagiotou, F. G. Moscoso, T. Lopes-Costa, J. M. Pedrosa and A. J. Tasiopoulos, *Inorg. Chem. Front.*, 2022, **9**, 4850–4863.

41 T. Xia, W. Cao, L. Guan, J. Zhang, F. Jiang, L. Yu and Y. Wan, *Dalton Trans.*, 2022, **51**, 5426–5433.

42 L. Yu, S. Ullah, K. Zhou, Q. Xia, H. Wang, S. Tu, J. Huang, H. L. Xia, X. Y. Liu, T. Thonhauser and J. Li, *J. Am. Chem. Soc.*, 2022, **144**, 3766–3770.

43 X. L. Lv, L. Feng, L. H. Xie, T. He, W. Wu, K. Y. Wang, G. Si, B. Wang, J. R. Li and H. C. Zhou, *J. Am. Chem. Soc.*, 2021, **143**, 2784–2791.

44 Y. F. Zhang, Q. Wang, D. X. Xue and J. Bai, *Inorg. Chem.*, 2020, **59**, 11233–11237.

45 Z. Duan, Y. Li, X. Xiao, X. Huang, X. Li, Y. Li, C. Zhang, H. Zhang, L. Li, Z. Lin, Y. Zhao and W. Huang, *ACS Appl. Mater. Interfaces*, 2020, **12**, 18715–18722.

46 F. Hu, Z. Di, M. Wu, M. Hong and J. Li, *Cryst. Growth Des.*, 2019, **19**, 6381–6387.

47 Y. Feng, X. Xin, Y. Zhang, B. Guo, F. Li, X. Kong, Y. Wang, X. Wang, Y. Wang, L. Zhang and D. Sun, *Cryst. Growth Des.*, 2019, **19**, 1509–1513.

48 H. Jiang, J. Jia, A. Shkurenko, Z. Chen, K. Adil, Y. Belmabkhout, L. J. Weselinski, A. H. Assen, D. X. Xue, M. O'Keeffe and M. Eddaoudi, *J. Am. Chem. Soc.*, 2018, **140**, 8858–8867.

49 L. Zhang, S. Yuan, L. Feng, B. I. Guo, J. U.-S. Qin, B. Xu, C. Lollar, D. Sun, H.-C. Zhou, L.-L. Zhang, B.-B. Guo, B. Xu, D.-F. Sun, S. Yuan, L. Feng, J.-S. Qin, C. Lollar and H.-C. Zhou, *Angew. Chem., Int. Ed.*, 2018, **57**, 5095–5099.

50 D. F. Sava Gallis, J. A. Harvey, C. J. Pearce, M. G. Hall, J. B. DeCoste, M. K. Kinnan and J. A. Greathouse, *J. Mater. Chem. A*, 2018, **6**, 3038–3045.

51 M. L. Gao, W. J. Wang, L. Liu, Z. B. Han, N. Wei, X. M. Cao and D. Q. Yuan, *Inorg. Chem.*, 2017, **56**, 511–517.

52 A. H. Assen, Y. Belmabkhout, K. Adil, P. M. Bhatt, D. X. Xue, H. Jiang and M. Eddaoudi, *Angew. Chem., Int. Ed.*, 2015, **54**, 14353–14358.

53 R. Luebke, Y. Belmabkhout, Ł. J. Weseliński, A. J. Cairns, M. Alkordi, G. Norton, Ł. Wojtas, K. Adil and M. Eddaoudi, *Chem. Sci.*, 2015, **6**, 4095–4102.

54 D. X. Xue, Y. Belmabkhout, O. Shekhah, H. Jiang, K. Adil, A. J. Cairns and M. Eddaoudi, *J. Am. Chem. Soc.*, 2015, **137**, 5034–5040.

55 J. P. Vizuet, M. L. Mortensen, A. L. Lewis, M. A. Wunch, H. R. Firouzi, G. T. McCandless and K. J. Balkus, *J. Am. Chem. Soc.*, 2021, **143**, 17995–18000.

56 M. S. Christian, K. J. Fritzsching, J. A. Harvey, D. F. Sava Gallis, T. M. Nenoff and J. M. Rimsza, *J. Am. Chem. Soc.*, 2022, **2**, 1889–1898.

57 Q. Li, X. Cai, L. H. Chen, B. bin Guan, Z. L. Fan, W. Zhu and D. X. Xue, *Inorg. Chem.*, 2021, **60**, 8143–8153.

58 P. M. Bhatt, Y. Belmabkhout, A. Cadiau, K. Adil, O. Shekhah, A. Shkurenko, L. J. Barbour and M. Eddaoudi, *J. Am. Chem. Soc.*, 2016, **138**, 9301–9307.

59 B. K. Ling, J. Li, Y. Q. Zhai, H. K. Hsu, Y. T. Chan, W. P. Chen, T. Han and Y. Z. Zheng, *Chem. Commun.*, 2020, **56**, 9130–9133.

60 *Per- and Polyfluorinated Substances (PFAS) Factsheet|National Biomonitoring Program|CDC*, **https://www.cdc.gov/biomonitoring/PFAS_FactSheet.html**, accessed 7 September 2022.

61 M. G. Evich, M. J. B. Davis, J. P. McCord, B. Acrey, J. A. Awkerman, D. R. U. Knappe, A. B. Lindstrom, T. F. Speth, C. Tebes-Stevens, M. J. Strynar, Z. Wang, E. J. Weber, W. M. Henderson and J. W. Washington, *Science*, 2022, **375**(6580), DOI: **10.1126/science.abg9065**.

62 I. T. Cousins, J. C. Dewitt, J. Glüge, G. Goldenman, D. Herzke, R. Lohmann, C. A. Ng, M. Scheringer and Z. Wang, *Environ. Sci.: Processes Impacts*, 2020, **22**, 2307–2312.

63 Y. Wen, Á. Rentería-Gómez, G. S. Day, M. F. Smith, T. H. Yan, R. O. K. Ozdemir, O. Gutierrez, V. K. Sharma, X. Ma and H. C. Zhou, *J. Am. Chem. Soc.*, 2022, **144**, 11840–11850.

64 J. T. Moore and C. C. Lu, *J. Am. Chem. Soc.*, 2020, **142**, 11641–11646.

65 *PFAS Explained|US EPA*, **https://www.epa.gov/pfas/pfas-explained**, accessed 7 September 2022.

66 J. H. Cavka, S. Jakobsen, U. Olsbye, N. Guillou, C. Lamberti, S. Bordiga and K. P. Lillerud, *J. Am. Chem. Soc.*, 2008, **130**, 13850–13851.

67 K. O. Christe and W. W. Wilson, *J. Fluorine Chem.*, 1990, **46**, 339–342.

68 M. Hudlicky, *J. Fluorine Chem.*, 1985, **28**, 461–472.

69 A. Zalkin and D. H. Templeton, *J. Am. Chem. Soc.*, 1953, **75**, 2453–2458.

70 K. M. Cole, D. W. Kirk and S. J. Thorpe, *Surf. Sci. Spectra*, 2020, **27**, 024010.